HAL
open science

The binary absorption coefficients for H 2 +CO 2 mixtures in the 2.12-2.35 μm spectral region determined by CRDS and by semi-empirical calculations

Didier Mondelain, C. Boulet, J.-M. Hartmann

To cite this version:

Didier Mondelain, C. Boulet, J.-M. Hartmann. The binary absorption coefficients for H 2 +CO 2 mixtures in the 2.12-2.35 μm spectral region determined by CRDS and by semi-empirical calculations. Journal of Quantitative Spectroscopy and Radiative Transfer, 2021, 260, pp.107454. 10.1016/j.jqsrt.2020.107454 . hal-03426922

HAL Id: hal-03426922

https://hal.science/hal-03426922v1

Submitted on 12 Nov 2021

HAL is a multi-disciplinary open access archive for the deposit and dissemination of scientific research documents, whether they are published or not. The documents may come from teaching and research institutions in France or abroad, or from public or private research centers.

L'archive ouverte pluridisciplinaire **HAL**, est destinée au dépôt et à la diffusion de documents scientifiques de niveau recherche, publiés ou non, émanant des établissements d'enseignement et de recherche français ou étrangers, des laboratoires publics ou privés.

The binary absorption coefficients for H_2+CO_2 mixtures in the 2.12-2.35 µm spectral region determined by CRDS and by semi-empirical calculations

D. Mondelain[a,*] C. Boulet[b], J.-M. Hartmann[c],

[a] Univ. Grenoble Alpes, CNRS, LIPhy, 38000 Grenoble, France

[b] Université Paris-Saclay, CNRS, Institut des Sciences Moléculaires d'Orsay (ISMO), 91405 Orsay, France

[c] Laboratoire de Météorologie Dynamique/IPSL, CNRS, Ecole Polytechnique, Institut polytechnique de Paris, Sorbonne Université, Ecole Normale Supérieure, PSL Research University, F-91120 Palaiseau, France

[*] Corresponding author: didier.mondelain@univ-grenoble-alpes.fr

Key words

Collision induced absorption; molecular hydrogen; carbon dioxide; CRDS

Abstract

Spectra of CO_2+H_2 mixtures have been recorded at room temperature by using the cavity ring down technique, for four spectral intervals in the 2.12-2.35 µm CO_2 spectral window which is within the (1-0) band of H_2. The binary coefficients $B_{CO_2-H_2} + B_{H_2-CO_2}$ have been retrieved from the spectra recorded at different pressures after subtraction of the CO_2 monomer contribution and of the H_2-H_2 and CO_2-CO_2 collision induced absorptions (CIAs). In order to reduce the uncertainties, new measurement of the pure H_2 CIA, the main subtracted contribution, at the percent level are also reported. The new set of experimental binary coefficients is compared to values provided by semi-empirical calculations made with the assumption of an isotropic CO_2-H_2 interaction potential and neglecting the short interaction-range induced electric dipole. This comparison shows the limits of using such a model, which is the only one available, in that spectral region.

1. Introduction

Geological elements like valley networks [1,2], high erosion rates [3,4], sediments [5], hydrated material [6] are strong proofs of the presence of liquid water at the surface of ancient Mars at multiple epochs and for extended periods of time. Even if the atmosphere of Mars, dominated by CO_2, was much denser than today (typically of a few bars), the greenhouse effect produced by the CO_2 molecule in addition to water is not sufficient to recreate, alone, surface temperatures above the melting point of water [7,8,9,10]. Several scenarios including the greenhouse effect of clouds [11,12,13,14], volcanism [15,16] or meteorite impacts [17,18,19,20], have thus been proposed to solve this enigma but without success so far.

It was recently shown that H_2 and CH_4 are the only known yet plausible gases that are susceptible to be at the origin of a sufficiently high surface temperature of the early-Martian atmosphere, compatible with liquid water through additional absorption induced by collision (CIA) with CO_2 molecules [21,22]. Because of the absence of measurements for H_2+CO_2 and CH_4+CO_2 CIAs at that time, their intensities and shapes were calculated in [22] from a linear combination of the known H_2+H_2 and CO_2+CO_2 CIAs with the spectrally integrated intensities of these new CIAs determined from *ab initio* calculations of the 0th order spectral moment. A little later, the first measurements of the H_2+CO_2 and CH_4+CO_2 CIAs have been made at room temperature, in the 50–550 cm^{-1} spectral range by Fourier transform spectroscopy [23] and they were very recently updated with reduced uncertainties [24]. These experimental results confirm the significantly stronger CIAs of H_2+CO_2 and CH_4+CO_2 when compared to the H_2+N_2 and CH_4+N_2 CIAs, as calculated in [22], but the measured shapes and intensities are found quite different from those predicted in [22].

In order to provide H_2+CO_2 and CH_4+CO_2 CIAs data over a broader spectral range (i.e. 0-1500 cm^{-1}) and at different temperatures (i.e. from 100K to 600K), semi-empirical calculations were also performed in [24]. More precisely, these calculations were based on the widely used "isotropic approximation". They provided the area-normalized spectral shape of the CIAs, which were then multiplied by the "true" integrated intensity calculated using the formalism developed in [25], allowing to fully account for the influence of the intermolecular potential anisotropy on the 0th order spectral moment of the band.

The aim of this paper is to provide additional experimental data for H_2+CO_2 CIA and to further test and refine this model. For that, a highly sensitive cavity ring down spectrometer (CRDS) is used to record spectra of H_2+CO_2 mixtures at room temperature in the 2.12-2.35 µm spectral region within the (1-0) band of H_2 as shown on **Figure 1**. Then, H_2-CO_2 binary absorption coefficients are extracted from these spectra, which requires the accurate knowledge of the subtracted H_2-H_2 CIA that we have also measured here. This experimental work is described in Sec. 2. The modeling of the H_2+CO_2 CIA is then described in Sec. 3 and compared to the experimental datasets before discussing perspectives of that work and concluding in Sec. 4.

2. Experimental binary coefficients

a. CRDS setup and spectra recordings

The CRDS setup used in this work has already been used for continua measurements of pure H_2O and CO_2 and for a mixture of H_2O in air [26,27,28,29]. Briefly, the light emitted by a distributed feedback (DFB) laser diode is sent into a high finesse cavity (finesse between 39 000 and 100 000 depending of the wave number) consisting in two mirrors with highly reflective coatings separated by 142 cm. The output mirror of this cavity is placed on a PZT tube allowing for dithering the cavity length and thus obtaining resonance between the light (at a fixed frequency) and a longitudinal mode of the optical cavity. At resonance, the laser light entering the cavity is switched off with an acousto-optic modulator. A signal, decreasing exponentially with time and corresponding to the decay time of photons leaking from the cavity [i.e. the ring down (RD) time, τ], is detected by a photodiode. The absorption coefficient of the gas sample, $\alpha(\nu)$, is then derived from the fitted RD time, at the laser frequency ν, with the following equation:

$$\alpha(\upsilon) = \frac{1}{c\tau(\upsilon)} \quad \frac{1}{c\tau_0(\upsilon)} \tag{1}$$

With c the speed of light and τ_0 the ring down time with the optical cavity filled with a non-absorbing gas.

The absorption spectra are recorded by a step-by-step change of the laser frequency obtained by changing the laser diode temperature, the injection current being fixed. During the spectra

acquisition, the laser frequency is permanently measured with a wavelength meter (model 621-A IR from Bristol). Four DFB laser diodes (from Nanoplus GmbH) were used in this work, centred respectively at 4250, 4435, 4522 and 4724 cm^{-1}. Two sets of mirrors from Layertec were installed successively in the cavity, optimized respectively for the 1.95-2.20 µm and the 2.20-2.50 µm spectral ranges.

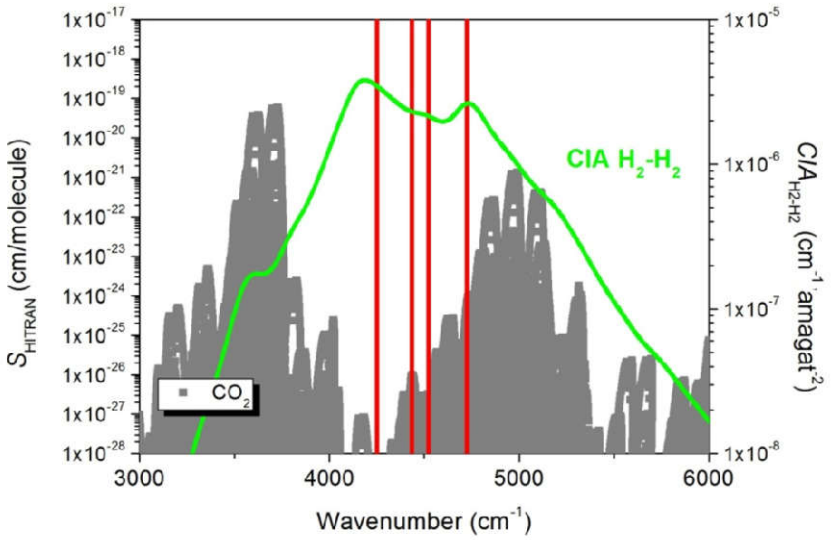

Figure 1. Overview of the H_2-H_2 CIA and of the CO_2 absorption lines provided by the HITRAN2016 database [30] in the region of the (1-0) band of H_2. The central wave numbers of the four DFB laser diodes used in this work are indicated by the vertical red solid lines.

A 1000 mbar pressure gauge (ATM.1ST from STS, accuracy of ±0.1% of the full scale) was connected to the cavity. The temperature of the CRDS cell was continuously monitored by a sensor (TSic 501 from IST, ±0.1 K accuracy) fixed on the external wall of the cavity underneath the enveloping thermal insulation foam. During the whole period of measurements the temperature varied between 296 K and 298 K.

Series of spectra were recorded for two mixtures of H_2+CO_2 with different fractions of H_2 (70.31% and 29.47%) known with a 2σ-relative uncertainty of 0.46% and 1.5%, respectively. For each laser diode and mixture, spectra were recorded at the different pressures summarized in ***Table 1***.

Central wavenumber in cm^{-1}	Pure H_2 in Torr	H_2(70%)-CO_2(30%) in Torr	H_2(30%)-CO_2(70%) in Torr
4250	280	280	280[a]
	200	200	200[a]
4430	400	340	400[a]
	280	280	280[a]
		200	
4525	400	700	600
	280	500	400
		300	
4720		300	150
		150	75
		75	

[a] *The presence of an unknown species in the H_2(30%)-CO_2(70%) mixture with numerous strong absorption lines prevents to accurately retrieve the binary coefficients for these diodes.*

Table 1. Pressure conditions used to record the CRDS spectra with the different laser diodes and gas mixtures.

For each total pressure, four spectra were recorded successively: one with the cell filled with argon, two with the targeted mixture and a last one with argon. The two argon spectra are used here to accurately determine the baseline (i.e. the ring down time τ_0), as this atom does not absorb, and to check its stability after pumping and filling cycles. An example illustrating this procedure is given in **Figure 2**. A baseline stability of the order of 10^{-10} cm^{-1} was achieved with the set of mirrors optimized between 1.95-2.20 µm (and used with the 4720 cm^{-1} and 4525 cm^{-1} laser diodes) while a stability of a few 10^{-9} cm^{-1} was observed with the other set of mirrors (used with the 4250 cm^{-1} and 4430 cm^{-1} laser diodes). The deterioration results from the fact that the coating of one of the mirrors was damaged, making the baseline more sensitive to changes of the mirrors alignment. Note that the minimal detectable absorption coefficient of our spectra, α_{min}, with the cell filled with argon, was around 2×10^{-10} cm^{-1} to 3×10^{-10} cm^{-1}.

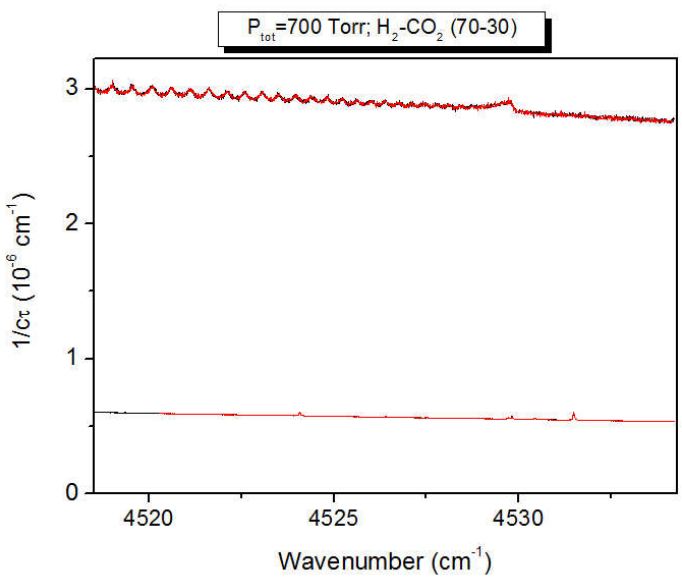

Figure 2. Ar and H_2+CO_2 spectra recorded at 700 Torr with the laser diode emitting around 4525 cm^{-1}. The Ar spectra (lower ones) correspond to the baseline which is subtracted to the H_2+CO_2 spectra (upper ones).

b. Extraction of the binary coefficients

The frequency axis of all the spectra was first refined using the positions of some absorption lines of water vapour, deduced from HITRAN2016 database [30], which is present in traces in the argon gas used (see **Figure 2**). The argon spectra are then fitted with a second order polynomial, after removing the water lines. This fitted baseline is then subtracted to the H_2+CO_2 spectra, leading to the determination of the absorption coefficient, *α (ν)*, which is then the sum of several terms:

$$\alpha(\nu,T) = M_{CO_2}\rho_{CO_2} + M_{H_2}\rho_{H_2} + B_{CO_2-CO_2}\rho_{CO_2}^2 + B_{H_2-H_2}\rho_{H_2}^2 + (B_{CO_2-H_2}+B_{H_2-CO_2})\rho_{CO_2}\rho_{H_2}$$

(Eq. 1)

Where $M_{CO_2}\rho_{CO_2}$ and $M_{H_2}\rho_{H_2}$ are the contributions due to the "monomer local lines" of CO_2 and H_2, respectively and ρ represents the density. B_{i-j} corresponds to the binary coefficient where *i* denotes the absorbing gas and *j* the perturber. These coefficients are generally given in cm^{-1} $amagat^{-2}$ units. Note that Rayleigh scattering does not appear in Eq. (1) since it is negligible under our experimental conditions for the spectral range studied here with a contribution of typically a few 10^{-10} cm^{-1} calculated from [31].

To retrieve the binary coefficients $B_{CO_2-H_2} + B_{H_2-CO_2}$ (indistinguishable experimentally) from *α(ν)*, it is necessary to subtract the other terms appearing in Eq. (1). For this, the local CO_2 monomer contribution was calculated from the HITRAN2016 database [30] using Voigt profiles truncated at ±25 cm^{-1} without including the pedestal for the absorption lines [32]. To better reproduce the CO_2 absorption lines it was necessary to multiply the air-broadening coefficients provided by the HITRAN2016 database by a factor 1.55 to take into account the fact that the collision partner is H_2 and not air.

According to HITRAN2016, only two H_2 lines are strong enough in our spectral range to make a detectable contribution in our spectra. These quadrupole electric transitions, belonging to the (1-0) vibrational band are the *S*(0) (ν_0=4497.8385 cm^{-1}; *S*(296K)=1.79×10^{-26} cm/molecule) and *S*(1) (ν_0=4712.9046 cm^{-1}; *S*(296 K)=3.19×10^{-26} cm/molecule) transitions (**Figure 5**). The first one is clearly too far from the spectral ranges covered by our laser diodes but the second one, situated at ~0.2 cm^{-1} from the lowest wavenumber of the spectral range covered by the 4720 cm^{-1} laser diode, is susceptible to contribute to the total absorption. Nevertheless, no such effect has been observed in the residual when not accounting for the H_2 monomer contribution as it will be discussed later. The $M_{H_2}\rho_{H_2}$ contribution is thus disregarded in our data analysis.

Here it must be noticed that, for the spectra recorded around 4250 cm^{-1}, the contribution of a few strong water vapor lines has to be subtracted as well as a very small contribution of N_2O for the spectra at 4430 cm^{-1} for the mixture with 70% of H_2. H_2O and N_2O were present at the 20 ppmv and 30 ppbv levels in the gas samples, respectively. More problematic is the presence of at least one unknown species, in the tank containing 30% of H_2 in CO_2, that absorbs in the spectral regions near 4250 cm^{-1} and 4430 cm^{-1}. As this species presents a relatively strong absorption with numerous absorption lines it was not possible to accurately retrieved the binary coefficients for these diodes using this gas mixture.

The CO_2 continuum contribution is evaluated using the absorption coefficient reported in Figure 3 of Ref. [33] for 20 amagat of CO_2 at room temperature. In order to use the measurements of [33], we have digitalized the spectrum displayed in Fig. 3 of [33] and subtracted the calculated contribution of the monomer for a density of 20 amagat at 296K. This "corrected" absorption coefficient, varying as the squared density, was divided by 400 $amagat^2$ and multiplied by our experimental CO_2 squared densities. The absorption contribution obtained in such a way was then subtracted to our spectra. Note that the binary CO_2 absorption coefficients $B_{CO_2-CO_2}$derived from [33] are in good agreement (within few percents) with the ones obtained from previous CRDS measurements in the 4320-4380 cm^{-1} spectral range [28].

Finally the contribution of the H_2-H_2 CIA was calculated using, in a first step , the binary coefficients provided at 300 K in HITRAN2016 [34], which are those calculated in Ref. [35]. These different removed contributions are shown in **Figure 3** for the absorption coefficient measured around 4525 cm^{-1} with a mixture of 70% of H_2 in CO_2 at a total pressure of 700 Torr. The main contribution among the subtracted ones is by far due to the H_2-H_2 CIA which has to be accurately determined. No error bars are provided neither in HITRAN nor in Ref. [35] for these binary coefficients. For this reason, we decided to measure the $B_{H_2-H_2}$ binary coefficients following the same procedure described above with argon. The pressure conditions of the recordings using pure H_2 (purity>99.9999% from Air Liquide) are given in ***Table 1***.

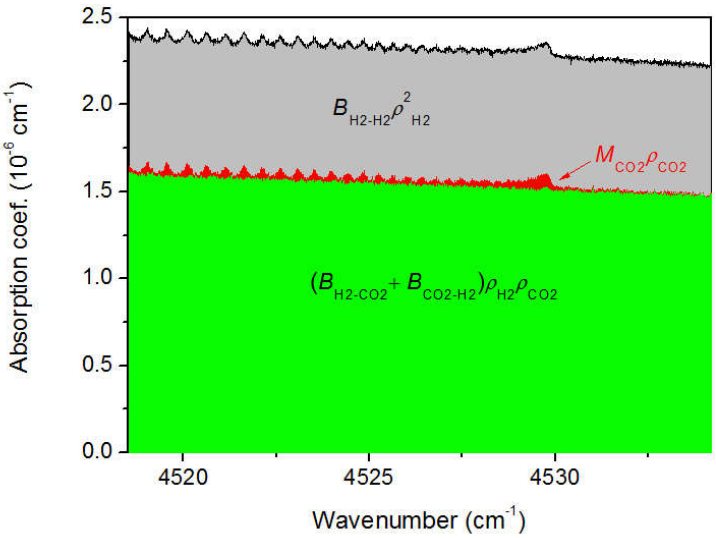

Figure 3. Presentation of the different contributions to the total absorption coefficient measured around 4525 cm^{-1} for a mixture of 70% of H_2 in CO_2 at a total pressure of 700 Torr. Refer to the text for the different notations. Note that the CO_2 continuum absorption, of the order of 6×10^{-10} cm^{-1}, is not shown.

The binary coefficients derived from the different pure H_2 spectra are plotted in **Figure 4** together with those given in HITRAN2016 database. For each diode, a very good agreement is observed between the binary coefficients retrieved from spectra recorded at different pressures, showing the reliability of our measurements. Our results, reported in the *Supplementary Material*, obtained with an uncertainty at the percent level or better, are systematically lower than the data in [35] by 3.6%, 6.9% and 3.4% near 4250 cm^{-1}, 4430 cm^{-1} and 4525 cm^{-1}, respectively (see **Table 2**). These differences seem compatible with uncertainties on the calculations due to numerical uncertainties of a few percent and the assumption of an isotropic H_2-H_2 interaction potential[1].

$B_{H_2-H_2}$ 10^{-6} cm^{-1} amagat^{-2}	**4250 cm^{-1}**	**4430 cm^{-1}**	**4525 cm^{-1}**
HITRAN2016	3.478	2.320	2.146
This work	3.353(29)	2.160(15)	2.072(30)

Table 2. Binary coefficients of pure H_2-H_2 CIA provided by HITRAN2016 and obtained in this work. The numbers in parenthesis represent the 1σ uncertainty in units of the last digit.

[1] These elements come from a discussion with the corresponding author of Ref. [35].

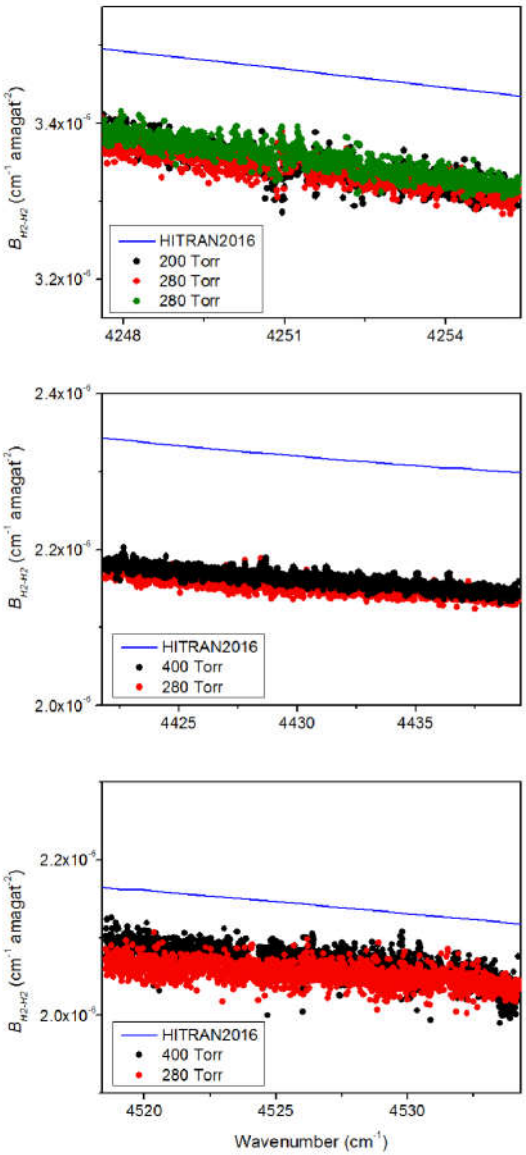

Figure 4. Binary coefficient of the H_2-H_2 CIA derived from spectra recorded at different pressures near 4250 cm^{-1} (upper panel), 4425 cm^{-1} (middle panel) and 4525 cm^{-1} (lower panel). The binary coefficients from HITRAN2016 database are plotted with blue solid lines.

The final binary coefficients $B_{CO_2-H_2} + B_{H_2-CO_2}$ (**Figure 5**) are thus derived using our experimental values for the CIA of H_2 and are reported in the *Supplementary Material*.

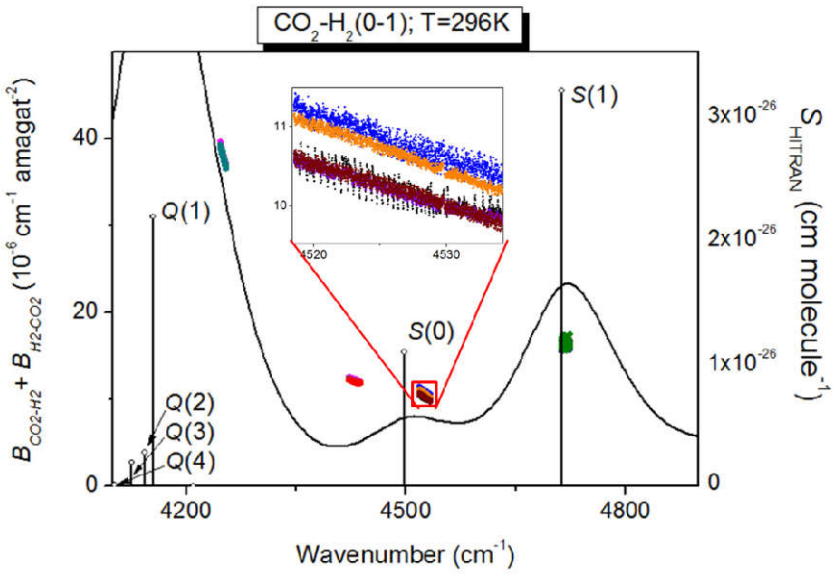

Figure 5. Overview of the experimental $\boldsymbol{B_{CO_2-H_2}} + \boldsymbol{B_{H_2-CO_2}}$ binary coefficients retrieved from the CRDS spectra recorded at different total pressures (corresponding to different colors) and the coefficients calculated using the semi-empirical model described in Sec. 3 (black solid line). The insert near 4525 cm^{-1} shows the systematic deviation observed for the binary coefficients retrieved from the two H_2+CO_2 mixtures. The intensities of the monomer given by HITRAN2016 is also shown together with the assignment of the different transitions.

c. *Estimated uncertainties on the experimental binary coefficients*

The uncertainties on the derived $B_{CO_2-H_2} + B_{H_2-CO_2}$ binary coefficients have been calculated with the error propagation approach using Eq. (1), assuming uncorrelated variables and neglecting Rayleigh absorption and the H_2 monomer absorption, $M_{H_2}\rho_{H_2}$.

The baseline stability was evaluated to be better than 1×10 ^{10} cm ^{1} for the laser diodes at 4720 cm^{-1} and 4525 cm^{-1}. For the laser diodes at 4430 cm^{-1} and 4250 cm^{-1}, the stability is degraded to 2×10 ^{9} cm ^{1} due to a damaged mirror (the mirrors were changed for these diodes). Temperatures and total pressures are measured with accuracies of δT=0.1K and δP=0.75 Torr (corresponding to $\delta P_{max}/P_{max}$=0.1%), respectively. The claimed uncertainties on the CO_2 and H_2 molar fractions are 1% and 0.46%, respectively for the mixture with 70% of H_2 and 0.65% and 1.5%, respectively for the mixture with 30% of H_2.

The monomer contribution uncertainties, δM_{CO2}, were determined by taking into account the error bars on the line intensities, self-broadening γ_{self}, air-broadening γ_{air} (from which the H_2 broadening is deduced (see above)) coefficients and CO_2 partial pressure. Four simulations, $\delta_i(\nu)$, were performed, each of them with either, the intensities, γ_{self} , γ_{air} or P_{CO2} values increased by their error bar. The uncertainty on δM_{CO2} was obtained from:

$$\delta M_{CO2}(\nu) = \left[\sum_{i=1}^{4} \delta_i(\nu)^2\right]^{1/2} \qquad \text{(Eq. 2)}$$

A conservative uncertainty of 2% was adopted on our measured CIA values from pure H_2 gas.

For the binary coefficient $B_{CO_2-CO_2}$ taken from [33], where no error bars is given, we estimated the uncertainty to 5% from comparison with binary coefficients determined from CRDS spectra in [28]. Nevertheless, it has to be underlined that the contribution of the CO_2 continuum is weak for all the studied spectral ranges so that a larger uncertainty would have a very limited impact on the final calculated uncertainties.

Once the final uncertainties were calculated for all the data points, we chose to remove the results with uncertainties larger than 5% which correspond to regions of strong absorption lines where the derivation of the binary coefficients is more difficult.

The uncertainty on the $B_{H_2-H_2}$ coefficients was determined in the same way from the simplified equation:

$$\alpha(\nu, T) = M_{H_2}\rho_{H_2} + B_{H_2-H_2}\rho_{H_2}^2 \qquad \text{(Eq. 3)}$$

As discussed above, the monomer contribution of H_2 is negligible in the spectral ranges studied here and the main contribution to the uncertainty comes from the base line stability.

Note that in our calculations of the local monomer absorption, a cutoff value of ±25 cm^{-1} was used. In order to test the sensitivity of the results to the choice of the cut-off distance, the value of 5 cm^{-1} was also used, leading to a marginal (per mil or lower) change on the binary coefficients retrieved from the spectra recorded with the diodes at 4250 cm^{-1}, 4430 cm^{-1} and 4525 cm^{-1}. In the case of the spectra obtained with the 4720 cm^{-1} laser diode, the largest change is 1.7%. The impact of including or not the plinth in the local monomer absorption is even lower. In any case this effect is not considered as a source of uncertainty and does not enter in the final estimated uncertainties calculated just above.

The final uncertainties adopted for the $B_{CO_2-H_2} + B_{H_2-CO_2}$ coefficients have nevertheless to be increased compared to the calculated ones as a systematic shift of 6.5% is observed near 4525 cm^{-1} between the binary coefficients retrieved from the two H_2+CO_2 mixtures (**Figure 5**) while, for a given mixture, the data points derived from spectra at different pressures are almost superimposed. This observation could not be confirmed for the other spectral intervals due to the presence of a non-identified interfering species for the H_2(30%)-CO_2(70%) mixture (at 4250 cm^{-1}, 4430 cm^{-1}) and a too strong CO_2 absorption (at 4720 cm^{-1}). This systematic shift probably comes from the fact that the CO_2 and H_2 abundances are not known with the accuracy claimed by the manufacturer. To be conservative, a final (1σ) uncertainty of 6.5% is adopted for all the $B_{CO_2-H_2} + B_{H_2-CO_2}$ coefficients.

These coefficients, plotted on **Figure 5**, constitute a set of data points useful to test the semi-empirical model developed in [24] and described below.

3. Semi-empirical calculations and comparison with experimental data

The CIA due to collisions between H_2 and CO_2 molecules retrieved from the experimental spectra can result from different contributions (or have different origins).

A contribution could come from the CO_2 molecule which has a vibrational transition within the spectral region investigated, while the H_2 molecule makes a pure rotational transition with the $j = 0$ selection rule due to the isotropic polarizability. However, from the integrated intensities given in Table 3 of [33] for the CO_2-CO_2 pair, $S_{CO2-CO2}$, it is possible to estimate the integrated intensities for the CIA bands of the CO_2-H_2 pair, S_{CO2-H2}, from the ratio of the polarizability matrix elements (i.e. $\frac{S_{CO2-H2}}{S_{CO2-CO2}} = \left(\frac{0|\alpha_{H2}|0}{00^00|\alpha_{CO2}|00^00}\right)^2 = \left(\frac{5.5}{19.8}\right)^2 = 6\ 10^{-3}$) or from the ratio of the quadrupole matrix element (i.e. $\frac{S_{CO2-H2}}{S_{CO2-CO2}} = \left(\frac{0|Q_{H2}|0}{00^00|Q_{CO2}|00^00}\right)^2 = \left(\frac{0.39}{3.19}\right)^2 = 1.5\ 10^{-2}$). For the strongest collision induced band, centered near 4390 cm^{-1}, the maximum value corresponds to $6.0\ 10^{-10}\ \mathrm{cm}^{-1}\ \mathrm{amagat}^{-2}$ which is negligible when compared to the observed binary coefficients in **Figure 5**.

The second contribution is the rotovibrational spectrum in which ro-vibrational transitions belonging to the 0-1 band of the H_2 molecule occur while the CO_2 molecule undergoes pure rotational transitions. This contribution is calculated using the model described below, and corresponds to the black solid line in **Figure 5**. In that case, the integrated intensity is estimated to about 3.7×10^{-2} cm^{-2} $amagat^{-2}$ which is 8 orders of magnitude larger than the previous contribution.

a. Calculation of the CO_2-H_2 (0-1) CIA band

The most rigorous approach for the calculation of the CIA spectrum of CO_2-H_2 pairs, in the region of the fundamental of H_2, should use a fully quantum theory taking into account both the anisotropy of the intermolecular potential and the short range components of the induced dipole (ID) (see for instance [36]). However, the large number of collisional channels which should be taken into account with CO_2 as a collisional partner prevents the use of that method. Moreover, nothing is known about the vibrational dependence of the short range components of the ID (remind that H_2 makes a 0-1 vibrational transition).

We have therefore adapted the semi-empirical model previously built for predicting the roto-translational CIA spectra for the CO_2-H_2 pair [24] to that new situation. Since details can be found in the appendix of [24], we give here only a brief summary of its mains assumptions.

The intermolecular potential: Among the reliable anisotropic potentials available for the CO_2-H_2 pair we have used that of Li *et al*. [37] that we previously used for the calculation [24] of the roto-translational spectra.

The induced dipole: As mentioned above, with no information available on its short range behavior, the ID has to be limited to its long range components. In the present work we have only considered the most significant ones, i.e. the quadrupolar (in R^{-4}) and hexadecapolar (in R^{-6}) induced components. They are specified by a set of four indices $\lambda_1, \lambda_2, \Lambda \wedge L$ satisfying some general constraints (see [38]) and determined by the transition matrix elements of the isotropic and anisotropic polarizability and the multipole moments of H_2 ($0|\alpha|1$, …) and the corresponding permanent polarizabilities and multipoles of CO_2 ($00^00|\alpha|00^00$, …). All these parameters are known and can be found in the literature (see [39] for H_2 and [40] for CO_2).

The isotropic approximation (IA): In that limit, one assumes that the potential can be limited to its isotropic component in the calculation of the pair distribution function. As a consequence the absorption coefficient can be written as a sum of rotational components, each having a purely translational profile:

$$\alpha_{iso}(\omega) = \frac{4\pi^2}{3\ c} n_0^2 \omega \left(1 \quad e^{-\ \omega/k_B T}\right) \sum_n \Gamma_n(T) G_n(\omega \quad \omega_n, T) \qquad \text{Eq. (4)}$$

n_0 is the number density at standard temperature and pressure (which corresponds to 1 amagat). Each component *n* is specified by a set of quantum numbers, $n = \{j_1, j_2, j'_1, j'_2, \lambda_1, \lambda_2, \Lambda \wedge L\}$. In this expression, j_i designates the rotational quantum number of CO_2 (*i*=1) or H_2 (*i*=2); a prime indicates final states. $\Gamma_n(T)$ represents the strength of the rotational component while $\omega_n = \omega_{j_1 \to j'_1} + \omega_{v2=0 j_2, v2=1 j'_2}$ is its central frequency. More details may be found in [41].

The translational profile $G_n(\omega \quad \omega_n, T)$ is exactly similar to that previously computed [24] for the roto-translational spectrum (since we neglect the vibrational dependence of the potential). Once the rotational strengths and the translational profile are available, the CIA spectrum, in the isotropic approximation, can be calculated and compared with the experimental data.

In the case of the roto-translational spectrum, the inadequacy of the isotropic approximation was clearly established [24] from the analysis of the spectral moments. Indeed, a formalism had been developed by Gruszka and Borysow [25] for the calculation of the 0th order spectral moments which fully accounts for the anisotropy of the potential. At 300 K, and for the roto-translational spectrum, the ratio of the "exact" 0th moment to that obtained within the isotropic approximation was 1.84 [24], demonstrating the failure of the latter. It was therefore of primary interest to make a similar comparison for the present case of the CO_2-H_2 (0-1) spectrum. Since we obtain, in this case, a ratio of 1.87 at 300K, it appears that the IA is also inadequate in this spectral region.

Therefore we have followed the same procedure used previously for the roto-translational spectrum [24]:

i) We assume that the area-normalized absorption profile, α_{iso}/S_{iso}, can be reasonably calculated within the IA.

ii) We multiply this normalized profile by the "true" anisotropic integrated intensity, S_{aniso} (remind that in this spectral region, the integrated intensity is proportional to the 0th order spectral moment), i.e.:

$$\alpha_{aniso}(\omega, T) = \frac{S_{aniso}(T)}{S_{iso}(T)} \ \alpha_{iso}(\omega, T)$$

With $\frac{S_{aniso}(296K)}{S_{iso}(296K)} = 1.87$

While this procedure led to a reasonable agreement with the experimental data for the roto-translational band [24], **Figure 5** here shows that it does not accurately describe the present experimental results. The theoretical absorption is larger than the experimental data points for some spectral ranges and smaller for some others.

Among the numerous and more or less justified assumptions made in the model, two deserve some comments and are susceptible to explain the observed differences:

- The neglect of the short range components of the ID. Indeed, their influence may be very different from that in the case of the roto-translational spectra, since now the H_2 partner makes a vibrational transition.
- The existence of mixed contributions in the spectral density which exist for anisotropic intermolecular interactions but disappear when the IA is used. With an anisotropic potential, the spectral density is a sum of terms arising from the autocorrelation of the spherical components of the ID (pure terms) *plus* terms arising from the correlation of different components (mixed terms) which do not exist within the IA. As demonstrated in [42], in the case of the roto-translational spectra of CO_2-Ar pairs, quadrupolar and hexadecapolar components do not mix within the IA while it is no more the case when the anisotropy of the potential is accounted for, invalidating the IA which underlies the present model. In other words, modeling the spectral line shape as an incoherent sum of contributions from pure spherical components may give a wrong estimate of the CIA.

4. Conclusion

In this work, the CRDS technique is used to record spectra of H_2+CO_2 mixtures around 4250 cm^{-1}, 4430 cm^{-1}, 4525 cm^{-1} and 4720 cm^{-1}. Thanks to its high base line stability, this technique is well adapted to measure continua absorption with reduced uncertainties as previously demonstrated [26,27,28,29]. The binary coefficients $B_{CO_2-H_2} + B_{H_2-CO_2}$ retrieved from spectra recorded at different pressures show a very good agreement for each spectral region. To reduce the uncertainties on these retrieved values, the CIA of H_2-H_2, which is the dominating subtracted contribution, is also accurately measured. The comparison of the experimental binary coefficients with the semi-empirical calculations (already used for the roto-translational spectrum) show that the

later, which is the only model available so far, are not able to accurately reproduce the experimental data. This is likely due to the (unavoidable) use of the isotropic approximation of the interaction potential and to the fact that short range components of the ID are not considered since unknown.

Acknowledgements

This work was performed in the frame of the ANR project *COMPLEAT* (ANR-19-CE31-0010-01).

References

[1] Carr MH. The martian drainage system and the origin of valley networks and fretted channels, J Geophys Res 1995;100:7479-7507. DOI: 10.1029/95JE00260

[2] Hynek B M, Beach M, Hoke MRT. Updated global map of Martian valley networks and implications for climate and hydrologic processes. J Geophys Res (Planets) 2010;115:E09008. DOI: 10.1029/2009JE003548

[3] Craddock RA, Howard AD. The case for rainfall on a warm, wet early Mars. J Geophys Res (Planets) 2002;107:5111. DOI: 10.1029/2001JE001505

[4] Quantin-Nataf C, Craddock RA, Dubuffet F, Lozac'h L, Martinot M. Decline of crater obliteration rates during early Martian history. Icarus 2019;317:427. DOI: 10.1016/j.icarus.2018.08.005

[5] Grotzinger JP, Gupta S, Malin MC, Rubin DM, Schieber J, Siebach K, Sumner DY, Stack KM, Vasavada AR, Arvidson RE, Calef F, Edgar L, Fischer WF, Grant JA, Griffes J, Kah LC, Lamb MP, Lewis KW, Mangold N, Minitti ME, Palucis M, Rice M, Williams RME, Yingst RA, Blake D, Blaney D, Conrad P, Crisp J, Dietrich WE, Dromart G, Edgett KS, Ewing RC, Gellert R, Hurowitz JA, Kocurek G, Mahaffy P, McBride MJ, McLennan SM, Mischna M, Ming D, Milliken R, Newsom H, Oehler D, Parker TJ, Vaniman D, Wiens RC, Wilson SA. Deposition, exhumation, and paleoclimate of an ancient lake deposit, Gale crater, Mars. Science 2015;350:7575. DOI: 10.1126/science.aac7575

[6] Ehlmann BL, Edwards CS. Mineralogy of the Martian Surface. Annual Review of Earth and Planetary Sciences 2014;42:291. DOI: 10.1146/annurev-earth-060313-055024

[7] Mishna M, Baker V, Milliken R, Richardson M and Lee C. Effects of obliquity and water vapor/trace gas greenhouses in the earky Martian climate, J Geophys Res 2013;118:1-17. DOI: 10.1002/jgre.20054

[8] Wordsworth R, Forget F, Eymet V. Infrared collision-induced and far-line absorption in dense CO_2 atmospheres, Icarus 2010;210:992-997. DOI: 10.1016/j.icarus.2010.06.010

[9] Wordsworth R, Forget F, Millour E, Head JW, Madeleine J-B, Charnay B. Global modelling of the early martian climate under a denser CO_2 atmosphere: Water cycle and ice evolution. Icarus 2013;222:1. DOI: 10.1016/j.icarus.2012.09.036

[10] Turbet M, Tran H. Comment on "Radiative Transfer in CO_2-Rich Atmospheres: 1. Collisional Line Mixing Implies a Colder Early Mars". J Geophys Res (Planets) 2017;122:2362. DOI: 10.1002/2017JE005373

[11] Forget F, Pierrehumbert RT. Warming early Mars with carbon dioxide clouds that scatter infrared radiation. Science 1997;278:1273-1276. DOI: 10.1126/science.278.5341.1273

[12] Wordsworth R, Forget F, Millour E, Head JW, Madeleine JB, Charnay B. Global modeling of the early Martian climate under denser CO2 atmosphere: Water cycle and ice evolution. Icarus 2013;222:1-19. DOI: 10.1016/j.icarus.2012.09.036

[13] Forget F, Wordsworth R, Millou E, Madeleine J-B, Kerber L, Leconte J, Marcq E, Haberle RM. 3D modeling of the early martian climate under a denser CO_2 atmosphere: Temperatures and CO_2 ice clouds. Icarus 2013;222: 81-99. DOI: 10.1016/j.icarus.2012.10.019

[14] Ramirez RM, Kasting JF. Could cirrus clouds have warmed early Mars?. Icarus 2017;281:248. DOI: 10.1016/j.icarus.2016.08.016
[15] Halevy I, Head JW. Episodic warming of early Mars by punctuated volcanism. Nature Geoscience 2014;7:865. DOI : 10.1038/ngeo2293
[16] Kerber L, Forget F, Wordsworth R. Sulfur in the early martian atmosphere revisited: Experiments with a 3-D Global Climate Model. Icarus 2015;261:133. DOI: 10.1016/j.icarus.2015.08.011
[17] Segura TL, Toon OB, Colaprete A and Zahnle K. Environmental effects of large impacts on Mars, Science 2002;298:1977-1980. DOI: 10.1126/science.1073586
[18] Segura TL, McKay CP and Toon OB, An impact-induced, stable, runaway climate on Mars, Icarus 2012;220: 144-148. DOI: 10.1016/j.icarus.2012.04.013
[19] Steakley K, Murphy J, Kahre M, Haberle R, Kling A. Testing the impact heating hypothesis for early Mars with a 3-D global climate model. Icarus 2019;330:169. DOI: 10.1016/j.icarus.2019.04.005
[20] Turbet M, Gillmann C, Forget F, Baudin B, Palumbo A, Head J, Karatekin O. The environmental effects of very large bolide impacts on early Mars explored with a hierarchy of numerical models. Icarus 2020;335:113419. DOI : 10.1016/j.icarus.2019.113419
[21] Ramirez R, Kopparapu R, Zugger M, Robinson TD, Freedman R, Kasting JF. Warming early Mars with CO_2 and H_2. Nature Geosci 2014;7:59–63. DOI: 10.1038/ngeo2000
[22] Wordsworth R, Kalugina Y, Lokshtanov S, Vigasin A, Ehlmann B, Head J, Sanders C, Wang H. Transient reducing greenhouse warming on early Mars. Geophys Res Lett 2017;44:665–671. DOI: 10.1002/2016GL071766
[23] Turbet M, Tran H, Pirali O, Forget F, Boulet C, Hartmann J-M. Far infrared measurements of absorptions by CH_4 + CO_2 and H_2 + CO_2 mixtures and implications for greenhouse warming on early Mars. Icarus 2019;321: 189–199. DOI: 10.1016/j.icarus.2018.11.021
[24] Turbet M, Boulet C, Karman T. Measurements and semi-empirical calculations of CO_2+CH_4 and CO_2+H_2 collision-induced absorption across a wide range of wavelengths and temperatures. Application for the prediction of early Mars surface temperature. Icarus 2020;346:113762. DOI: 10.1016/j.icarus.2020.113762.
[25] Gruszka M, Borysow A. New analysis of the spectral moments of collision induced absorption in gaseous N_2 and CO_2. Mol Phys 1996;88:1173-1185. DOI: 10.1080/00268979609484502
[26] Lechevallier L, Vasilchenko S, Grilli R, Mondelain D, Romanini D, Campargue A. The water vapour self-continuum absorption in the infrared atmospheric windows: new laser measurements near 3.3 and 2.0 µm. Atmos Meas Tech 2018;11:2159–2171. DOI: 10.5194/amt-11-2159-2018
[27] Richard L, Vasilchenko S, Mondelain D, Ventrillard I, Romanini D, Campargue A. Water vapor self-continuum absorption measurements in the 4.0 and 2.1 µm transparency windows. J Quant Spectrosc Radiat Transfer 2017;201:171–179. DOI: 10.1016/j.jqsrt.2017.06.037
[28] Mondelain D, Vasilchenko S, Čermák P, Kassi S, Campargue A. The CO_2 absorption spectrum in the 2.3 µm transparency window by high sensitivity CRDS: (II) Self-absorption continuum. J Quant Spectrosc Radiat Transfer 2017;187:38–43. DOI: 10.1016/j.jqsrt.2016.09.003
[29] Vasilchenko S, Campargue A, Kassi S, Mondelain D. The water vapour self- and foreign-continua in the 1.6 µm and 2.3 µm windows by CRDS at room temperature. J Quant Spectrosc Radiat Transfer 2019;227:230–238. DOI: 10.1016/j.jqsrt.2019.02.016
[30] Gordon IE, Rothman LS, Hill C, Kochanov RV, Tan Y, Bernath PF, Birk M, Boudon V, Campargue A, Chance KV, Drouin BJ, Flaud JM, Gamache RR, Hodges JT, Jacquemart D, Perevalov, VI, Perrin A, Shine KP, Smith MAH, Tennyson J, Toon GC, Tran H, Tyuterev VG, Barbe A, Császár, AG, Devi VM, Furtenbacher T, Harrison JJ, Hartmann J-M, Jolly A, Johnson TJ, Karman T, Kleiner, I, Kyuberis AA, Loos J, Lyulin OM, Massie ST, Mikhailenko SN, Moazzen-Ahmadi N, Müller HSP, Naumenko OV, Nikitin AV, Polyansky OL, Rey M, Rotger M, Sharpe SW, Sung K, Starikova E, Tashkun SA, Vander Auwera J, Wagner G, Wilzewski J, Wcisło P, Yu S, Zak EJ. The HITRAN2016 Molecular Spectroscopic Database. J Quant Spectrosc Radiat Transf 2017;203:3-69. DOI: 10.1016/j.jqsrt.2017.06.038.
[31] Thalman R, Zarzana K, Tolbert MA, Volkamer R. Rayleigh scattering cross-section measurements of nitrogen, argon, oxygen and air. J Quant Spectrosc Radiat Transf 2014;147:171–7. DOI: 10.1016/j.jqsrt.2014.05.030
[32] Ptashnik IV, McPheat RA, Shine KP, Smith KM, Williams RG. Water vapor self-continuum absorption in near-infrared windows derived from laboratory measurements. J Geophys Res 2011;116:D16305. DOI: 10.1029/2011JD015603.
[33] Tonkov MV, Filippov NN, Bertsev VV, Bouanich JP, Van Thanh Nguyen, Brodbeck C. Measurements and empirical modeling of pure CO_2 absorption in the 2.3 µm region at room temperature: far wings, allowed and collision-induced bands. Appl Opt 1996; 35:4863–70.

[34] Karman T, Gordon IE, van der Avoird A, Baranov YI, Boulet C, Drouin BJ, Groenenboom CG, Gustafsson M, Hartmann J-M, Kurucz RL, Rothman LS, Sun K, Sung K, Thalman R, Tran H, Wishnow EH, Wordsworth R, Vigasin AA, Volkamer R, van der Zande WJ. Update of the HITRAN collision-induced absorption section. Icarus 2019;328:160-175. DOI: 10.1016/j.icarus.2019.02.034
[35] Abel M, Frommhold L, Li X, Hunt KLC. Collision-Induced Absorption by H_2 Pairs: From Hundreds to Thousands of Kelvin. J Phys Chem A 2011;115:6805–6812. DOI: 10.1021/jp109441f
[36] Karman T, Miliordos E, Hunt KLC, Groenenboom GC, van der Avoird A. Quantum mechanical calculation of the collision-induced absorption spectra of N_2-N_2 with anisotropic interaction. J Chem Phys 2015;142:084306. DOI: 10.1063/1.4907917
[37] Li H, Roy PN, Le Roy RJ. Analytic Morse/long range potential energy surfaces and predicted infrared spectra for CO_2-H_2. J Chem Phys 2010 ;132:214309. DOI: 10.1063/1.3428619
[38] Poll JD, Hunt JL. On the moments of the pressure induced spectra of gases. Can J Phys 1976;54:461-470. DOI: 10.1139/p76-052
[39] Meyer W, Borysow A, Frommhold L. Absorption spectra of H_2-H_2 pairs in the fundamental band. Phys Rev A 1989;40:6931-6949. DOI: 10.1103/PhysRevA.40.6931
[40] Hartmann J-M, Boulet C, Jacquemart D. Molecular dynamics simulations for CO_2 spectra. II. The far infrared collision-induced absorption band. J Chem Phys 2011;134:094316. DOI: 10.1063/1.3557681
[41] Boissoles J, Tipping RH, Boulet C. Theoretical study of the collision induced fundamental absorption spectra of N_2-N_2 pairs for temperatures between 77 and 297 K. J Quant Spectrosc Radiat Transfer 1994;51: 615-627. DOI: 10.1016/0022-4073(94)90115-5
[42] Borysow A, Moraldi M. The role of the anisotropic interaction on collision induced absorption of systems containing linear molecules: The CO_2–Ar case. J Chem Phys 1993;99:8424-8429. DOI: 10.1063/1.465618